*Journal of Thermal Analysis and Calorimetry, Vol. 71 (2003) 915–925*

# COMBUSTION DERIVED ULTRAFINE $\gamma$-$Fe_2O_3$ Structure, morphology and thermal studies

*N. N. Mallikarjuna, B. Govindaraj, Arunkumar Lagashetty and A. Venkataraman*[*]

Department of Chemistry, Gulbarga University, Gulbarga-585 106, India

## Abstract

A novel combustion method of employing poly(ethylene glycol) with the precursor in a fixed ratio for the synthesis of ultrafine $\gamma$-$Fe_2O_3$ through a self-propagating combustion synthesis is reported. Four different precursors viz. ferrous hydroxide, ferrous oxalate dihydrate, ferric 8-hydroxyquinoline and ferric acetylacetonate are employed in this study for the conversion of these precursors to ultrafine $\gamma$-$Fe_2O_3$ particles. The as synthesized $\gamma$-$Fe_2O_3$ samples are characterized by XRD, SEM and thermal techniques. A case study for the synthesis of $\gamma$-$Fe_2O_3$ employing ferric acetyl acetonate as precursor is reported. The importance of employing thermal analysis techniques in understanding the combustion synthesis is envisaged.

**Keywords**: poly(ethylene glycol), precursors, self-propagating combustion reaction, thermal and structural studies, ultrafine $\gamma$-$Fe_2O_3$

## Introduction

Maghemite has attracted technological interest due to its magnetic and catalytic properties. Interest has increased following the observation that the properties are strongly dependent on the size of particles with dramatic changes when ultrafine/nanometric sizes are acquired [1–6]. The new synthetic routes for the preparation of ultrafine $\gamma$-$Fe_2O_3$ are under constant investigation and some of them include the ion-exchange reaction in $\alpha$-$NaFeO_2$ with benzoic acid [7], co-precipitation [8], thermal decomposition of metal hydrazine complexes [9], through a wet chemical synthesis of successive hydrolysis, oxidation and dehydration of ferrous chloride to obtain as small as 5 nm particles [10], selective oxidation of $Fe^{2+}$ and $Fe^{3+}$ [11], thermal decomposition of lipodocracite from solid solutions [12], thermal decomposition of metal carboxylate under the controlled conditions [13], and through ore beneficiation [14]. The porous nanosized iron oxide films prepared by the polymer precursor method using polyvinyl alcohol [15]. Many of these methods involved in the synthesis of $\gamma$-$Fe_2O_3$ are tedious, some of them time consuming with many reaction steps and often in many cases a small quantity of the material could be synthesised. Knowledge of the formation of the final product from its precursors through the use of thermal analysis

* Author for correspondence: E-mail: raman_chem@reddifmail.com.

*1388–6150/2003/ $ 20.00*
*Akadémiai Kiadó, Budapest*

techniques has gained importance in understanding the synthesis of materials [16–19].

Present investigation is a continuation of new synthetic routes using new precursors for the synthesis of ultrafine monophasic γ-$Fe_2O_3$. In the present study we have employed four different precursors viz. ferrous hydroxide, ferrous oxalate dihydrate, ferric 8-hydroxyquinoline, ferric acetylacetonate along with polyethylene glycol as an oxidant in a fixed ratio of 1:5 through a self-propagation combustion reaction.

It is reported in literature that poly(vinyl alcohol) can be employed as an oxidizing agent along with urea for the synthesis of other spinel ferrites through the combustion of citrate precursor [20]. However, this technique has some limitations viz., use of urea as a fuel, and also that poly(vinyl alcohol) has a wide variation of molecular masses, both of these parameters would influence the combustion to undergo as a highly exothermic reaction. Hence a new fuel which can also work as a controllable oxidant in a combustible reaction generating self-propagation is essential. In search of a suitable economic oxidant generating a self-propagating reaction, our use of poly(ethylene glycol) has given promising results in case of α-$Fe_2O_3$ to γ-$Fe_2O_3$ conversion [21]. In present investigation we report the synthesis of γ-$Fe_2O_3$ by employing poly(ethylene glycol), which acts as a reducing agent in the initial stage and this is followed with oxidation in the final combustion process. The as synthesized γ-$Fe_2O_3$ samples are then characterized by employing the thermal, structural, and scanning electron microscopy techniques. The thermal behavior of the combustion process employing ferric acetylacetonate precursor as an example is considered in detail for understanding the possible process and progress of the self-propagating combustion reaction. This thermal study is also undertaken in two different atmospheres viz. dynamic $O_2$ and $N_2$ to understand the effect of atmosphere.

## Experimental

Poly(ethylene glycol) with molecular mass 4.000 was obtained commercially. All the other chemicals employed were AR grade.

### *Preparation*

The precursors ferrous hydroxide, ferrous oxalate dihydrate, ferric 8-hydroxyquinoline and ferric acetylacetonate were prepared as reported elsewhere [23]. The above four precursors were mixed with poly(ethylene glycol) in the mass ratio 1:5 and ground together in a mortar. The resultant solids were placed in a silica crucible and heated in the air using a Bunsen burner. It was observed that poly(ethylene glycol) first melts, forms froths and ignites to form γ-$Fe_2O_3$ as residue. On cooling the residue to room temperature no traces of carbon impurities were observed. This reaction which occurs with the evolution of lot of gases and ignites autocatalytically is called a strong self-propagating combustion reaction, as it resembles the strong combustion reaction for the preparation of $SnO_2$ [24]. As this reaction is fast i.e., going to completion within 2–3 min, and ignites autocatalytically, the exact temperature of the

reaction could not be measured. However using a thermocouple the highest temperature of the reaction was found to be around 500°C. Thermal analysis traces for the reaction is explained in the later section. The γ-$Fe_2O_3$ samples obtained from the precursors viz., ferrous hydroxide ferrous oxalate dihydrate, ferric 8-hydroxy quinoline and ferric acetylacetonate in the present study are henceforth designated as $NM_1$, $NM_2$, $NM_3$ and $NM_4$ samples respectively.

*Characterization*

The thermal analysis curves were obtained from the Mettler Toledo Star instrument or polymer laboratories STA/1500 under static air, dynamic $O_2$ and dynamic dry nitrogen from room temperature to 800°C, with a heating rate of 10°C $min^{-1}$. The flow rate under the two dynamic atmospheres was 100 mL $min^{-1}$. The powder X-ray diffraction patterns were obtained from GEOL JDX-8P or SEIMEN (Japan) X-ray diffractometer using $CoK_\alpha$ radiation and the indexing was done by employing PROSZKI program. The morphology of the maghemite (γ-$Fe_2O_3$) samples were obtained on Leica Cambridge-440 scanning electron microscopy.

## Result and discussion

*Particle morphology*

The particle morphology of γ-$Fe_2O_3$ samples is shown in Figs 1a–d with the help of scanning electron micrographs. Following observation are made from the SEM images:

Figure 1a shows the SEM image of $NM_1$ sample. This image shows the interconnected ultrafine γ-$Fe_2O_3$ particles with nanosized dimensions forming agglomerates. Most of the particles are spherical. The structure of this material shows particles (<0.1 μm) and conchoidal fracture surfaces. The distribution of small particles was irregular but could not have arisen through a nucleation and growth reaction.

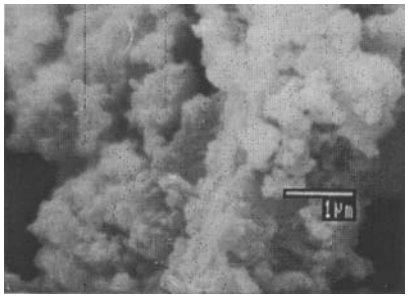

**Fig. 1a** SEM micrograph of γ-$Fe_2O_3$ prepared from ferrous hydroxide precursor ($NM_1$)

Figure 1b shows the SEM image of $NM_2$ sample. The particles are spherical and joined together to form chains of different dimensions. Joints as necking between the particles are also observed. A few agglomerates of particles of fine γ-$Fe_2O_3$ with non-chained structure are also observed.

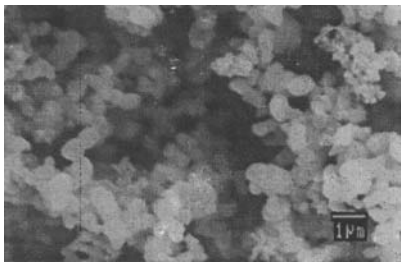

**Fig. 1b** SEM micrograph of γ-$Fe_2O_3$ prepared from ferrous oxalate dihydrate precursor ($NM_2$)

Figure 1ci shows the SEM image of $NM_3$ sample under low resolution. Ultrafine γ-$Fe_2O_3$ particles <100 nm, size are observed. In this figure it is also observed a dense and a very closely packed bamboo-like fiber of γ-$Fe_2O_3$ particles. On closer observation under high resolution (1 μm) shown in Fig. 1cii, some cracks are seen on the surface of this bamboo-like fiber, which might have resulted from the internal strains developed by the excess gases liberated during the combustion process. This bamboo-like structure indicates a self-assembly of nanosized γ-$Fe_2O_3$ particles. The bamboo-like fiber observed in here is similar to the MgO fiber reported elsewhere [25]. The difference in the present study is that the γ-$Fe_2O_3$ surface is not smooth when compared with the MgO fiber.

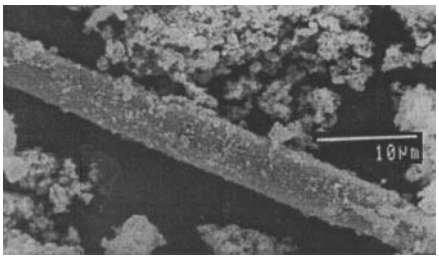

**Fig. 1ci** SEM micrograph of γ-$Fe_2O_3$ prepared from ferric 8-hydroxyquinoline precursor ($NM_3$) (low resolution)

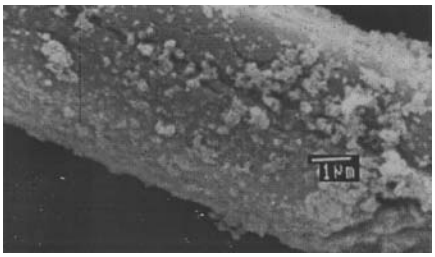

**Fig. 1cii** SEM micrograph of γ-$Fe_2O_3$ prepared from ferric 8-hydroxyquinoline precursor ($NM_3$) (high resolution)

Figure 1d shows the SEM image of $NM_4$ sample. This image shows very closely knitted continuous chains in three dimensions. On comparison between Fig. 1b, this figure shows a much better image of the particle packing and morphology.

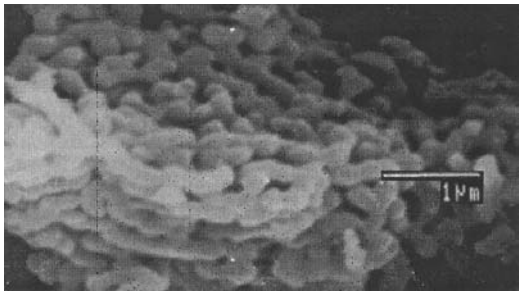


**Fig. 1d** SEM micrograph of γ-$Fe_2O_3$ prepared from ferric acetylacetonate precursor ($NM_4$)

It is observed from the above SEM images, that different precursors under the same experimental conditions for synthesis of γ-$Fe_2O_3$ gave different particle morphology. Some similarity is observed in $NM_2$ and $NM_4$ samples with the presence of chain like structures. However, $NM_4$ sample shows clear three-dimensional knitting of closed packed γ-$Fe_2O_3$ particles. The $NM_3$ sample shows a large bamboo-like fiber, with some surface cracking while the $NM_1$ sample showed a conchoidal fracture surface. It may be envisaged from these SEM images that the role of precursor is important in deciding the particle morphology of the final product.

On the basis of these SEM images, it is observed that $NM_4$ sample shows a better particle morphology for its possible application as a heterogeneous catalyst.

From the textural observations in Figs 1a–d, we conclude that comprehensive fusion does not occur. Careful examination of these images revealed no evidence of intracrystalline melting. However in case of sample $NM_4$ some general indications are that, the reaction preceded by a nucleation and growth process as noticed in any reaction interface, this image has resemblance with the SEM image for the $Ni_1C_{0.6}$ obtained by the thermal decomposition of nickel acetate [26].

It is also observed from literature that understanding the thermal behavior of the reaction path helps in envisaging the particle morphology of the final product [27]. The thermal behaviour of ferric acetylacetonate and the synthesis of γ-$Fe_2O_3$ from the precursor was carried out as a case study in the light of the above mentioned interesting aspects of $NM_4$ sample.

*Thermal analysis*

Figure 2 shows the DTA traces of $NM_1$, $NM_2$, $NM_3$ and $NM_4$ samples. The traces are taken under a static air atmosphere and the results are tabulated in Table 1. The endothermic peak at 64 and its shoulder at 88°C for $NM_1$ sample correspond to the loss of absorbed water molecules on the γ-$Fe_2O_3$ sample in two steps. A strong endothermic peak at 98°C corresponds to the loss of absorbed water molecule for $NM_4$ sample. It is believed that the storage and liberation of energy with regard to deformation and annealing are the important features in understanding the solid state reactions. The recovery or recrystallisation being the main energy releasing process of deformed solids has been investigated exclusively on metals and calcium carbonates [28]. In this

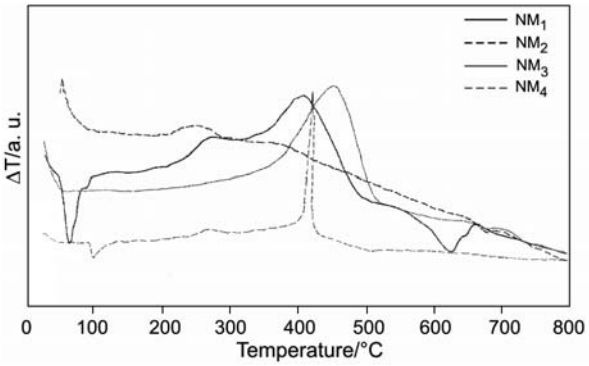


**Fig. 2** DTA traces of $NM_1$, $NM_2$, $NM_3$ and $NM_4$ samples under static air atmosphere

**Table 1** Characteristics of DTA traces of as synthesized γ-$Fe_2O_3$ samples

| Sample code | Endothermic peak/°C | Exothermic peak/°C |
|---|---|---|
| $NM_1$ | 64(s), 88(sh), 626(w) | 269(w), 400(b), 661(w) |
| $NM_2$ | 657(w) | 242(bw) |
| $NM_3$ | – | 446(vb), 692(w) |
| $NM_4$ | 98(w) | 269(bw), 419(s) |

s=strong, w=weak, b=broad, vb=very broad, bw=broad and weak, sh=shoulder

Fig. 2 the exothermic peaks observed at 269°C for $NM_1$ and $NM_4$ samples, and the exothermic peak at 269°C for $NM_4$ sample correspond to the recrystallisation of γ-$Fe_2O_3$ i.e., a change from cubic to tetragonal crystal system, which is in accordance with the similar observations reported elsewhere [28]. The broad exothermic peak around 400 for $NM_1$, around 242 for $NM_2$, 446 for $NM_3$ and a very sharp peak around 419°C for $NM_4$ samples correspond to the γ→α transition (γ-$Fe_2O_3$→α-$Fe_2O_3$ transition). This transition was confirmed from the X-ray diffraction patterns of isothermally heated $NM_1$ and $NM_2$ samples at 400, and 245 respectively, $NM_3$ sample at 450 and $NM_4$ sample at 420°C under a static air atmosphere for two hours each, which showed the α-$Fe_2O_3$ pattern in each case. The successive endothermic and exothermic peaks at higher temperature i.e., at 627, and 662 for $NM_1$ and 658 for $NM_2$ and 693°C for $NM_3$ samples correspond to the crystal structure changes taking place in the α-$Fe_2O_3$ samples, as α-$Fe_2O_3$ is found to exist in different crystal forms (e.g. rhombohedral, hexagonal etc.). However in the $NM_4$ sample the recrystallisation of α-$Fe_2O_3$ formed was not prominently observed on the DTA trace.

Now, on comparison of the above DTA traces, the following features are observed:

– Dehydration is observed for $NM_1$ and $NM_4$ samples. However, the process of dehydration in these two cases seems to be different, due to the presence of shoulder for the main peak in $NM_1$ sample.

– The recrystallisation from cubic to tetragonal crystal system is observed for $NM_1$ and $NM_4$ and not observed for $NM_2$ and $NM_3$ samples.

– Here, γ→α transition is observed for all the samples and in case of $NM_4$ sample, this transition is well defined.

– The phase changes of α–$Fe_2O_3$ is observed for the $NM_1$, $NM_2$ and $NM_3$ samples with the presence of weak exothermic and endothermic peaks. While the phase change was not observed in case of $NM_4$ sample.

Looking into the above DTA traces, it is strongly felt that the $NM_4$ sample that shows a well-defined dehydration and γ→α transition is a suitable example for the case study for the synthesis of γ–$Fe_2O_3$. It is also a well-known fact that the particle morphology plays an important role on the shapes of the DTA traces. The effect of these variations in shape and size of $NM_1$ to $NM_4$ samples as observed in Figs 1a–d have resulted in the changes in the shape index of DTA traces as shown in Fig. 2.

For the synthesis and stabilization of a well-defined γ-$Fe_2O_3$, the presence of water and along with the particle favourabe morphology is found to be essential. $NM_4$ sample in the present study has a clear dehydration step as noticed from the thermal traces and favorable particle morphology and size as observed on the SEM images. The lower γ→α-$Fe_2O_3$ transformation temperature for $NM_2$ sample and the higher γ→α-$Fe_2O_3$ transformation temperature for $NM_3$ sample might then be due to the absence of water of hydration in the former case and the favorable particle morphology in the later case.

It is important to understand the progress of thermal decomposition of the precursor i.e. ferric acetylacetonate for the study of its decomposed products. It is also essential to understand the thermal behavior of ferric acetylacetonate with poly(ethylene glycol) in the fixed ratio of 1:5 respectively for obtaining γ-$Fe_2O_3$ ($NM_4$ sample). This study of mixing ferric acetylacetonate with poly(ethylene glycol) is undertaken under two different atmospheres viz. dynamic $O_2$ and $N_2$ to understand the effect of atmosphere and these results are discussed.

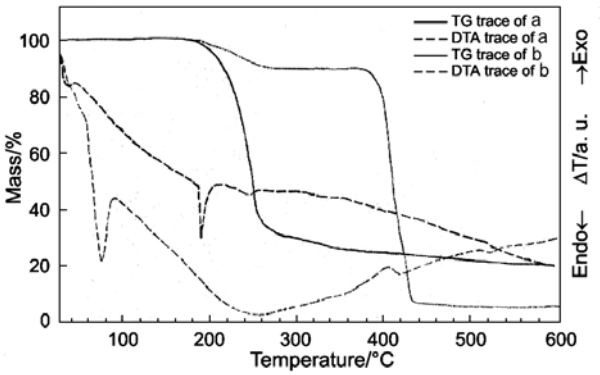


**Fig. 3 a** – TG/DTA trace of ferric acetyl acetonate under dynamic nitrogen atmosphere.
**b** – TG/DTA trace of ferric acetyl acetonate + PEG (1:5 mass ratio) under dynamic nitrogen atmosphere

Figure 3a shows the TG/DTA trace for ferric acetylacetonate precursor under dynamic nitrogen atmosphere. The characteristics of TG/DTA traces are given in Table 2. The final mass loss of 80% corresponds to the decomposition of ferric acetylacetonate to form α–$Fe_2O_3$ as residue. In the Fig. 3a the TG trace shows two stages of mass loss. The first mass loss starts at 175 and ends at 290°C. This stage resembles a sinusoidal curve indicating that the early and later stages of the process have slow rates and correspond to partial decomposition of ferric acetyl-acetonate complex. The second step follows the first step immediately and it is seen as a very slow process starting at 295 and ending at 400°C. The DTA trace shows two endothermic peaks at 199 and 246°C respectively, followed by a very broad and an unending (upto 600°C) endothermic peak.

**Table 2** Characteristics of DTA/TG traces of ferric acetylacetonate (FAC) and ferric acetylacetonate+poly(ethylene glycol) (PEG)

| Sample | Step | TG $T$/°C | | DTA $T$/°C | |
|---|---|---|---|---|---|
| | | start | end | endothermic | exothermic |
| FAC | I | 175 | 290 | 199, 246, 600 | – |
| Under $N_2$ atmosphere | II | 295 | 400 | | |
| FAC+PEG | I | 170 | 278 | 64, 255, 419 | – |
| Under $N_2$ atmosphere | II | 280 | 440 | | |
| FAC+PEG Under $O_2$ atmosphere | | 30 | 330 | – | 179, 219, 318, 210(sh), 280(sh) |

The Fig. 3b shows the TG/DTA trace for ferric acetylacetonate mixed with poly(ethylene glycol) in the ratio 1:5 under dynamic flow of $N_2$ atmosphere (with the flow rate 100 mL $min^{-1}$). The TG trace shows a clear two-step mass loss. The first step mass loss starts at 170 and ends at 278°C. The nature of this step resembles the first step mass loss observed for only ferric acetylacetonate shown in the Fig. 3a. However, the mass loss observed here is only 10.5 as compared to 69.5%. The second step of mass loss of 84% is observed as a steady process from 280 to 440°C. Thereafter there is no further decrease in the mass up to 600°C. The DTA trace shows a strong endothermic peak at 64°C and a very broad endothermic peak around 255°C. The third endothermic peak is observed at 419°C. The first endothermic peak at 64°C corresponds to the melting of poly(ethylene glycol). The formation of γ-$Fe_2O_3$ is completed at 419°C with the presence of third endothermic peak. The TG trace also supports the DTA trace indicating the partial decomposition of ferric acetylacetonate in the first step and a simultaneous decomposition of poly(ethylene glycol) and a partially decomposed ferric acetylacetonate in the second step.

To understand the effect of atmosphere on thermal behavior of the mixture (ferric acetylacetonate+poly(ethylene glycol)), we report the thermal traces under dynamic $O_2$ atmosphere.

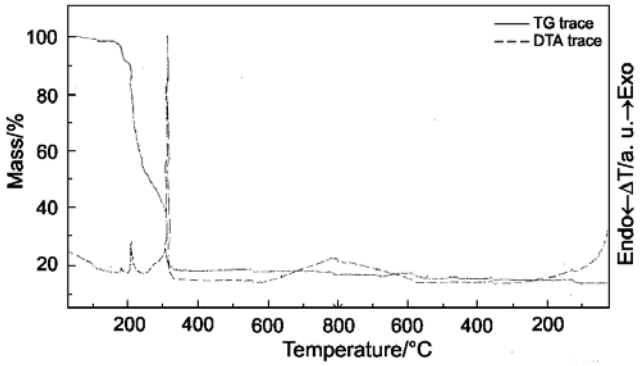


**Fig. 3c** TG/DTA trace of ferric acetylacetonate+PEG (1:5 mass ratio) on heating and cooling under dynamic $O_2$ atmosphere

Figure 3c shows the heating and cooling traces for the mixture of ferric acetylacetonate and poly(ethylene glycol) (of mass ratio 1:5) under the dynamic flow of $O_2$ atmosphere (flow rate 100 mL $min^{-1}$). TG traces show a complex multistep mass loss starting from the room temperature itself. The mass loss is completed at 330°C. Thereafter the TG trace shows no further loss in the mass upto 60°C and on cooling a slight irregular behavior is seen. The DTA trace shows three main exothermic peaks at 179, 219 and 318°C with shoulders at 210 and 280°C for the peak at 219 and 318°C, respectively. The TG and DTA traces observed here are different when they are compared with the Fig. 3a. The melting of poly(ethylene glycol) is not observed but the exothermic reaction involved in the oxidative decomposition of poly(ethylene glycol) with ferric acetylacetonate is observed along with the presence of these exothermic peaks. The complexities of the DTA trace is supported by the complicated multistep decomposition process in the TG trace. In this regard, it may be understood that the $O_2$ atmosphere plays a major role by reacting with poly(ethylene glycol) and ferric acetylacetonate mixture. The poly(ethylene glycol) without the aid of dynamic flow of $O_2$ decomposes the ferric acetylacetonate to obtain predominantly γ-$Fe_2O_3$ peaks resembling $NM_4$ sample (Fig. 4d). Hence, the mechanisms under the two atmospheres are different and the final oxide obtained in Fig. 3c is α-$Fe_2O_3$.

*X-ray diffraction*

Figures 4a–d shows the XRD pattern of samples $NM_1$, $NM_2$, $NM_3$ and $NM_4$ respectively. It is observed that all these patterns show cubic crystal system. These XRD data are compared with the ASTM file number 4-0755 for cubic system. The lattice spacing of $NM_1$, $NM_2$, $NM_3$ and $NM_4$ samples are 8.02, 8.04, 8.21 and 8.30 respectively. In case of $NM_1$ and $NM_2$ samples, the lattice spacing is almost same, and in

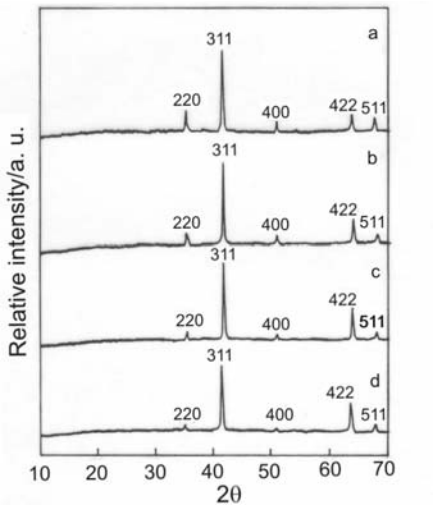


**Fig. 4** XRD patterns of $NM_1$, $NM_2$, $NM_3$ and $NM_4$ samples

$NM_3$ and $NM_4$, the values slightly vary. The slight changes in the lattice constant depend upon the history of the sample and precursor used.

## Conclusions

The following generalized conclusions may be made from this present study.

The use of poly(ethylene glycol) as a fuel and as a controllable oxidant in the synthesis of ultrafine γ-$Fe_2O_3$ particles suggests that this combustion route is novel and could be applied for synthesis of other ferrite materials. Also, the synthesis of γ-$Fe_2O_3$ takes place without going through any of the highly exothermic reactions to achieve ultrafine well-dispersed and high dense γ-$Fe_2O_3$ particles within a few minutes. However, fixing the proper mass ratio of poly(ethylene glycol) and the precursor is essential for obtaining good quality ultrafine monophasic γ-$Fe_2O_3$. It is observed from the present study that the particle morphology of the γ-$Fe_2O_3$ samples is influenced by the precursor taken. Hence, it is possible to tailor-make a given morphology of the final product with proper choice of the precursor. The thermal study (employing TG/DTA techniques) suggests that the phase transition from γ-$Fe_2O_3$ to α-$Fe_2O_3$ was also governed by particle morphology. The thermal traces also direct us in understanding the process and possible mechanism of self-propagating combustion reaction in a generalized way.

* * *

The authors are thankful to Prof. C. N. R. Rao President of theThird World Academy of Sciences, JNCASR, Bangalore, for his valuable help and suggestions. N. N. Mallikarjuna, B. Govindaraj and Arunkumar Lagashetty are thankful to the U.G.C., New Delhi for financial support. Thanks are to the Chairman, Department of Chemistry, Gulbarga University, Gulbarga for providing the laboratory facilities.

## References


1 Q. Li and Y. Wei, Mater. Res. Bull., 33 (1998) 779.
2 S. N. Vaidya, Bull. Mater. Sci., 22 (1999) 287.
3 R. D. Zysler, D. Fiorani and A. M. Testa, J. Mag. Mag. Mater., 224 (2001) 5.
4 R. H. Kodama, J. Mag. Mag. Mater., 200 (1999) 359.
5 N. Herron and D. L. Thorn, Adv. Mater., 10 (1998) 1173.
6 F. M. Pavel and A. M. Raymond, Langmuir, 16 (2000) 8568.
7 M. C. Blesa, E. Moran, J. D. Tornero, N. Menendez, E. Mata-Zamora and J. M.Saniger, J. Mater. Chem., 9 (1999) 227.
8 M. P. Morales, S. V. Verdaguer, M. I. Montero, C. J. Serna, A. Roig, L. Casas, B. Martinez and F. Sandiumenge, Chem. Mater., 11 (1999) 3058.
9 K. Suresh, N. R. S. Kumar and K. C. Patil, Adv. Mater., 3 (1991) 148.
10 G. Ennas, G. Marongiu, A. Musinu, A. Falqui, P. Ballirano and C. Caminiti, J. Mater. Res., 14 (1999) 1570.
11 N. J. Cherepy, D. B. Liston, J. A. Lovejoy, H. Deng and J. Z. Zhang, J. Phys. Chem., B 102 (1998) 770.
12 G. S. Chopra, C. Real, M. D. Alcala, L. Pérez-Maqueda and J. M. Subrtcria, Chem. Mater., 11 (1999) 1128.
13 M. M. Rahman and A. Venkataraman, J. Therm. Anal. Cal., 68 (2002) 91.
14 K. S. Rane, V. M. S. Vernekar and P. Y. Sawanth, Bull. Mater. Sci., 24 (2001) 331.
15 N. Uekawa and K. Kaneko, J. Phys. Chem. B, 102 (1998) 8719.
16 N. N. Mallikarjuna and A. Venkataraman, J. Therm. Anal. Cal., 68 (2002) 901.
17 V. Carles, P. Alphonse, P. Tailhades and A. Rousset, Thermochim. Acta, 334 (1999) 107.
18 A. Gholinia and F. R. Sale, J. Thermal Anal., 42 (1994) 733.
19 N. N. Mallikarjuna, A. Lagashetty and A. Venkataraman, J. Therm. Anal. Cal., (Communicated).
20 H. Ochiai and O. Kimura, Preparation of ferrites by the amorphous citrate process. Proceedings of the VI$^{th}$ International Conference on Ferrites (ICF-6), Tokyo and Kyoto, Japan 1992, p. 93.
21 A. Venkataraman, V. A. Hiremath, S. K. Date and S. D. Kulkarni, Bull. Mater. Sci., 24 (2001) 101.
22 N. N. Mallikarjuna and A.Venkataraman, Ind. J. Eng. Mat. Sci., (Communicated).
23 A. I. Vogel, 'Quantitative Inorganic Analysis', ELBS Longman, London 1979.
24 L. Fraigi, D. G. Lamas and N. E. Walsoe de Reca, Nanostruct. Mater., 11 (1999) 311.
25 G. Kordas, J. Mater. Chem., 10 (2000) 1157.
26 A. K. Galwey, S. G. Mackee, T. R. B. Mitchell, M. E. Brown and A. F. Bean, Reactivity of Solids, 6 (1988) 173.
27 M. E. Brown, R. H. M. Cross, K. C. Sole and M. W. Beck, Electron microscopy society of South Africa proceedings, 14 (1984) 153.
28 J. Mamoru Senna, J. Appl. Phys., 49 (1978) 4580.